PACS numbers: 42.55.Px; 42.60.Fc
DOI: 10.1070/QE2015v045n07ABEH015670

Frequency modulation of semiconductor disk laser pulses

I.O. Zolotovskii, D.A. Korobko, O.G. Okhotnikov

Abstract. **A numerical model is constructed for a semiconductor disk laser mode-locked by a semiconductor saturable absorber mirror (SESAM), and the effect that the phase modulation caused by gain and absorption saturation in the semiconductor has on pulse generation is examined. The results demonstrate that, in a laser cavity with sufficient second-order dispersion, alternating-sign frequency modulation of pulses can be compensated for. We also examine a model for tuning the dispersion in the cavity of a disk laser using a Gires–Tournois interferometer with limited third-order dispersion.**

Keywords: *semiconductor disk laser, frequency modulation of pulses.*

1. Introduction

Recent years have seen intense interest in semiconductor lasers that take advantage of an active semiconductor mirror and a cavity external relative to it. Such light sources are referred to as 'disk lasers' [1–3]. Their advantages include good heat removal from the gain element (which reduces the thermal lensing effect), high beam quality and the possibility of stable lasing in a wide range of pump powers. Moreover, a unique combination of properties is possible in the case of disk lasers: an ultrashort pulse duration and high pulse repetition rate at a relatively high average power [4–6]. It is also worth noting that disk lasers have a lower saturation energy than do solid-state and fibre lasers and, hence, are not susceptible to the effect of low-frequency instabilities even at low pulse energies [7].

For pulsed operation, disk lasers are most frequently mode-locked by semiconductor saturable absorber mirrors (SESAMs) [8], which enable the generation of pulses down to hundreds of femtoseconds in duration. High pulse repetition rates (up to 10 GHz and above) are ensured by the large gain bandwidth and the small cavity length (10 cm or shorter) of the disk lasers, with the possibility of taking advantage of harmonic mode locking. Its mechanism is based on gain saturation and recovery processes, which may lead to a pulse-interval-dependent time shift between pulses. As a result of this interaction, the pulses are spaced equidistantly along the length of the cavity [9, 10].

The above features of the disk lasers have a negative effect as well: their low gain saturation energy (in comparison with solid-state and fibre lasers) leads to considerable gain variations during each pulse and causes significant frequency modulation (FM) and spectral broadening of the pulses. It is important to note that the FM of the pulses is nonlinear, which makes it impossible to effectively reduce it using linear optical components (prisms and others). Nonlinear modulation leads to an asymmetric distortion of the pulse envelope and significantly degrades the quality of the pulses, and the impact of these negative factors increases with increasing pulse energy [11, 12].

In this paper, using numerical modelling we analyse the development of a nonlinear FM of semiconductor disk laser pulses and examine the possibility of suppressing alternating-sign FM using dispersion factors. In addition, we consider a numerical model for tuning the dispersion in the cavity of a laser based on an absorbing Gires–Tournois interferometer that has necessary dispersion characteristics, including a limited maximum third-order dispersion coefficient.

2. Model

Consider a model for a semiconductor disk laser schematised in Fig. 1. Lasing and amplification occur in an active semiconductor mirror under pumping. The laser cavity is formed by a semiconductor saturable absorber mirror (SESAM) and a partially transparent mirror as an output coupler.

The numerical model used in this study is similar to models reported previously [10, 13, 14]. It describes the evolution of an optical field with a complex amplitude $A(\tilde{z},t)$ in the

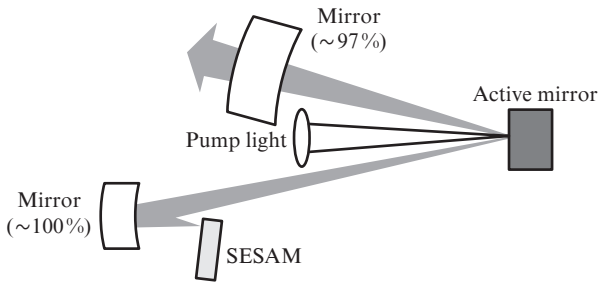

Figure 1. Schematic of the cavity of a semiconductor disk laser.

I.O. Zolotovskii, D.A. Korobko Ulyanovsk State University, ul. L. Tolstogo 42, 432017 Ulyanovsk, Russia; e-mail: rafzol.14@mail.ru, korobkotam@rambler.ru;
O.G. Okhotnikov Ulyanovsk State University, ul. L. Tolstogo 42, 432017 Ulyanovsk, Russia; present address: Optoelectronics Research Centre, Tampere University of Technology, Korkeakoulunkatu 3, 33101 Tampere, Finland; e-mail: oleg.okhotnikov@tut.fi

Received 9 September 2014; revision received 4 December 2014
Kvantovaya Elektronika **45** (7) 628–634 (2015)
Translated by O.M. Tsarev

laser cavity. The $\tilde{z}_g$ and $\tilde{z}_s$ coordinates correspond to the active and absorbing mirrors. The interaction of the field with the active mirror can be described using the single-pass power gain, and the gain saturation process is represented by a standard rate equation:

$$\frac{dg_s}{dt} = \frac{g_0 - g_s}{\tau_g} - \frac{g_s |A(\tilde{z}_g, t)|^2}{E_g}, \quad (1)$$

where $A(\tilde{z}_g, t)$ is the field amplitude at the active mirror input; $g_0(t)$ is the small-signal gain; $g_s(t)$ is the saturated gain; τ_g is the gain recovery time; and E_g is the gain saturation energy. A similar equation can be written for the saturable absorption $q(t)$ of the SESAM:

$$\frac{dq}{dt} = \frac{q_0 - q}{\tau_s} - \frac{q |A(\tilde{z}_s, t)|^2}{E_s}, \quad (2)$$

where q_0 is the absorption modulation depth; τ_s is the recovery time of the saturable absorber; and E_s is its saturation energy. For ~1 ps and longer pulses, the rate equations (1) and (2) provide an adequate approximation. Nonlinear phase changes can then be described by a phenomenological linewidth enhancement factor, α. In this approximation, the nonlinear term in the phase is proportional to the dimensionless gain $g_s(t)$ and modulation depth $q(t)$ [15, 16]. As a result, light propagation through the active mirror and SESAM can be described by the relations

$$\begin{aligned} A_{out}(\tilde{z}_g, t) &= \frac{g_s(t)}{2} A(\tilde{z}_g, t) \exp[i\alpha_g g_s(t)/2], \\ A_{out}(\tilde{z}_s, t) &= [1 - q(t)/2] A(\tilde{z}_s, t) \exp[-i\alpha_s q(t)/2]. \end{aligned} \quad (3)$$

The output coupling loss is taken into account by the output coupler reflectivity r, and the other losses, by the coefficient l. The peak gain wavelength is taken to be 1065 nm, typical of GaInAs/GaAs quantum well gain structures [13]. The finite gain bandwidth is modelled in the time domain using the spectral transfer function of the cavity

$$\tilde{A}_{out}(\omega) = \tilde{A}_{in}(\omega) \exp[-(\omega - \omega_0)^2/\omega_g^2], \quad (4)$$

where ω_g is the gain bandwidth and the frequency ω_0 corresponds to the peak gain wavelength λ_0. Dispersion characteristics were left out of consideration in the first stage. Their effect on the lasing process will be considered in the next section. The following parameters were used in the simulation: E_g = 75 nJ, E_s = 1 nJ, α_s = 1, α_g = 4, τ_g = 1 ns, τ_s = 5 ps, r = 0.97, q_0 = 0.02, l = 0.01. The above recovery times τ_g and τ_s, single-pass unsaturated gain g_0 and modulation depth q_0 are typical of semiconductor elements in disk lasers [3, 14]. The parameters α_s and α_g are identical to those reported previously [9, 13]. The saturation energy of the SESAM, E_s, corresponds to a saturation fluence of ~50 mJ cm^{-2} and mode spot diameter of 50 μm, and the saturation energy of the active mirror, E_g, corresponds to a saturation fluence of ~160 mJ cm^{-2} and mode spot diameter of 250 μm. Low-amplitude white noise was chosen as initial field conditions. We considered a problem with periodic boundary conditions in a simulation box 100 ps in width, which corresponded to a fundamental cavity frequency of 10 GHz.

The simulation results indicate that, when the gain g_0 exceeds a certain threshold, a pulse is generated from the initial noise. After 1000 to 1500 cavity passes, repetitively pulsed operation sets in, in which the pulse parameters change by less than 1% in each pass. With increasing g_0, the pulse energy increases. Note that, with increasing gain, the maximum in the spectrum of the pulse shifts to longer wavelengths, which indicates that the frequency modulation rate (sometimes referred to as a 'pulse chirp') depends on the gain. Such behaviour is exhibited by most disk lasers [10, 13]. When g_0 reaches the next threshold value, a second pulse is generated in the cavity. In the course of evolution (after 20 000 to 30 000 passes), gain saturation and recovery lead to equalisation of the characteristics of the pulses and cause them to be spaced equidistantly in the cavity [10]. As the gain increases and the next threshold values are reached, a third and other pulses are generated. The characteristics of the pulses are determined to a significant degree by the gain bandwidth ω_g. This dependence will be considered below. In what follows, g_0 is taken to be ~1 dB, which corresponds to a single pulse in the simulation box.

Consider a pulse generated in a laser at a gain bandwidth $\omega_g = 10^{13}$ s^{-1} [Fig. 2d, curve (*1*)]. If there is no phase modulation, i.e. $\alpha_s, \alpha_g = 0$, the carrier frequency of the pulse coincides with the peak gain frequency ω_0. Figure 2a shows the absorption $q(t)$ and gain $g_s(t)$ around the pulse, which determine the local phase shift $\Delta\varphi(t) = \alpha_g g_s(t)/2 - \alpha_s q(t)/2$ per pass. From the shape of $q(t)$ and $g_s(t)$, one can find the instantaneous frequency shift $\omega(t) - \omega_0$ induced by a single interaction of the pulse with the active and absorbing mirrors under the effect of the phase modulation: $\omega(t) = d\Delta\varphi(t)/dt$. The shifts are shown in Fig. 2b.

In the case of multiple cavity passes, the pulse is influenced by several factors. In the time domain, the envelope shifts towards the maximum in gain and the minimum in absorption (the rates of these processes are proportional to $\partial g_s/\partial t$ and $\partial q/\partial t$). In the spectral domain, the gain is highest at frequencies near ω_0. Spectral regions with large $\omega - \omega_0$ differences are filtered off. As a result, monotonic FM of the pulse can be observed, concentrated in a comparatively narrow spectral range [Fig. 2c, curve (*1*)]. Note that the pulse has a regularly shaped envelope and that the FM near its maximum is almost linear, which enables output pulse compression, e.g. using a diffraction grating pair.

In the case of a larger gain bandwidth [curves (*2*), (*3*)], reduced filtration leads to nonmonotonic FM (Fig. 2c). Pulse evolution during multiple cavity passes is accompanied by a cyclic process: formation of nonmonotonic FM, distortion of the envelope as a consequence of its shift to the maximum in gain and filtration in the region corresponding to the maximum shift of the instantaneous frequency [Figs 2c, 2d, curves (*3*)]. The cycle ends with the absorption of part of the pulse at its flat trailing edge and energy transfer to its leading edge. In experiments, the variation in the shape of the envelope shows up as a time variation of the autocorrelation trace of the pulse [14].

It is seen from the inset in Fig. 2 that nonmonotonic FM distorts the spectrum of the pulse as well. In the case of strong filtration [curve (*1*)] and monotonic FM, there is a one-to-one correspondence between the peak position of the pulse and the position of the maximum in the spectrum of the pulse, Ω_m. Note in this context that, with increasing gain and corresponding FM, the maximum in the spectrum shifts to longer wavelengths. As mentioned above, such behaviour is observed experimentally for most disk lasers. In the case of nonmonotonic FM, both the envelope and spectral density of the pulse are distorted, and there is no one-to-one correspondence between the instantaneous frequency at the peak posi-

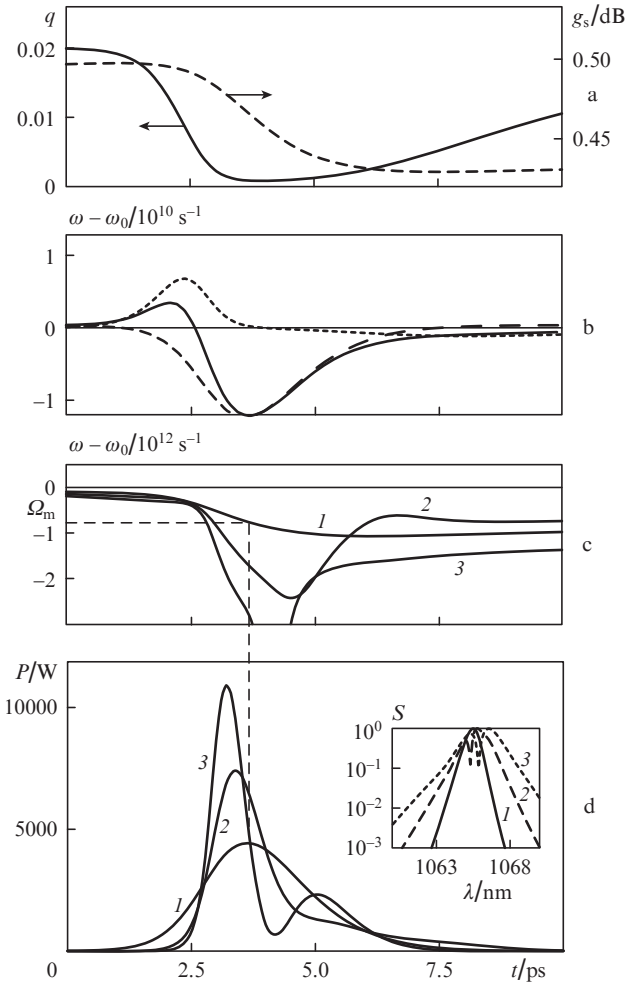

Figure 2. (a) Absorption $q(t)$, gain $g_s(t)$, (b) time dependences of the instantaneous pulse frequency shift induced by a single interaction with the saturable absorber (short-dashed line) and active mirror (long-dashed line), total frequency change per pass (solid line), (c) time dependences of the instantaneous pulse frequency and (d) pulse envelopes (P) after 30 000 cavity passes. Inset: $S(\lambda)$ spectra of pulses. The gain bandwidth is ω_g = (a, b) 10^{13}, (c, d) (*1*) 10^{13}, (*2*) 2×10^{13} and (*3*) 3×10^{13} s^{-1}.

tion and the maximum in the spectrum. One conclusion that can be drawn from the present simulation results is that strong spectral filtration improves the quality of disk laser pulses and, at the same time, reduces the pulse peak power and increases the pulse duration.

3. Cavity dispersion optimisation

Standard methods of intracavity dispersion compensation in pulsed lasers are aimed at reducing the total cavity dispersion in order to prevent dispersion-induced broadening and excessive FM of pulses. These methods imply the use of specific components having dispersion of opposite sign to that of the laser gain element. Use is typically made of dispersion-compensating fibres, e.g. photonic crystal fibres, or bulk dispersing elements, such as prisms, diffraction gratings and chirped mirrors [17–19]. In the case under consideration, the dispersion mechanism should eliminate differently directed FM of disk laser pulses. This can be achieved with both normal and anomalous cavity dispersion.

In a normal-dispersion cavity, a pulse becomes frequency-modulated: its instantaneous frequency increases with pulse duration. Such FM will be referred to as positive. By contrast, nonlinear phase modulation typically leads to negative FM of pulses (Fig. 2c). The normal cavity dispersion needed for negative FM compensation can be estimated from considerations that are used in describing the formation of a soliton pulse [14]. The stability of a fundamental soliton is known to be ensured by FM compensation due to nonlinear self-phase modulation and anomalous dispersion. In the case of a disk laser pulse, the situation is the same, to within the sign of FM: normal dispersion is needed for negative FM compensation. Given that in the case of complete FM the spectral width of a pulse is only determined by its duration τ, we can write an expression analogous to that describing a fundamental soliton:

$$4\pi^2\beta_2/\tau^2 = \Delta\Phi_{nl} = \alpha_g\Delta g_s/2 - \alpha_s\Delta q/2, \quad (5)$$

where β_2 is the normal dispersion of the cavity and Δg_s and Δq are the changes in saturated gain and saturable absorption during a pulse, which ensure negative FM. The nonlinear phase change per pass is several hundredths of a radian (Fig. 2), so the normal dispersion for pulse durations of the order of a picosecond is about 10^{-27}–10^{-26} s^2.

Nonmonotonic FM of a pulse can also be suppressed in the case of anomalous cavity dispersion. However, it should then be taken into account that anomalous dispersion suppresses positive FM and increases negative FM. A relation analogous to (5) has the form

$$\beta_2\Delta\omega^2 = \Delta\Phi_{nl} = \alpha_g\Delta g_s'/2 - \alpha_s\Delta q'/2, \quad (6)$$

where $\Delta g_s'$ and $\Delta q'$ are the changes in gain and saturable absorption, which determine positive FM. The spectral width of the frequency-modulated pulse meets the inequality $\Delta\omega > 2\pi/\tau$. Moreover, the suppressed positive FM is weaker than that above. Thus, to eliminate alternating-sign FM of a pulse, the magnitude of anomalous dispersion β_2 should be smaller than that in the case of a normal-dispersion cavity.

The present simulation results indicate that, with the above parameters, normal cavity dispersion $\beta_2 = 3.5\times10^{-27}$ s^2 ensures complete negative FM compensation. A pulse generated under such conditions is essentially transform-limited, and its instantaneous frequency differs from the peak gain frequency ω_0 by -3×10^{12} s^{-1} (~1.7 nm). A cavity with an anomalous dispersion $\beta_2 = -2\times10^{-27}$ s^2 ensures pulse generation with sufficiently uniform negative FM. Near the pulse maximum, FM is then almost linear, suggesting that further external pulse compression is possible. The spectral shape of the pulse is characteristic of frequency-modulated pulses with a maximum shifted to longer wavelengths. Note that, upon an increase in the magnitude of cavity dispersion β_2 (both normal and anomalous), dispersion-induced broadening leads to an increase in pulse duration and a decrease in pulse peak power.

4. Dispersion compensators based on Gires–Tournois interferometers

Consider the possibilities of controlling the cavity dispersion of a disk laser by tuning the characteristics of the active and absorbing mirrors; i.e. we will not touch on dispersion management with the use of specially designed prisms or chirped mirrors. The dispersion properties of the active mirror and SESAM are determined primarily by the microcavity formed

by a 100% Bragg reflector in its base and an outer coating of reflectivity $r_g < 1$, with a semiconductor structure in between. Depending on whether an amplifying or absorbing medium is located between the microcavity walls, the Bragg reflector forms an active or absorbing Gires–Tournois interferometer [20, 21]. The amplitude reflection coefficient of the interferometer is given by

$$R = \frac{r_g - a\exp(i\omega T)}{1 - ar_g\exp(i\omega T)}, \quad (7)$$

where T is the microcavity round-trip time (dependent on the angle of incidence of light) and a is absorption (gain). From $\Phi(\omega) = \arg R$ phase characteristics, one can extract data on the dispersion characteristics of the reflector: group delay time, dispersion and third-order dispersion (TOD):

$$\tau_d(\omega) = \partial\Phi/\partial\omega,\ \beta_2(\omega) = \partial^2\Phi/\partial\omega^2,\ \beta_3(\omega) = \partial^3\Phi/\partial\omega^3. \quad (8)$$

It is worth noting that the delay time τ_d and other dispersion characteristics for frequency-modulated pulses differ from those calculated using the simple relations (8) and depend as well on the FM of the pulse and the position of the maximum in its spectrum relative to the $|R(\omega)|$ reflection spectrum [22]. This dependence is, however, most pronounced when the spectrum of the pulse is well away from the midgap region, where $|R(\omega)|$ has high values. In the case under consideration, the centre frequency of the reflection spectrum approaches the frequency corresponding to the maximum in the spectrum of the pulse, which allows the dependence of the dispersion characteristics (8) on FM rate to be left out of consideration.

It is worth noting that Gires–Tournois interferometers with a semiconductor absorber are widely used for dispersion compensation. An interferometer can then be used as both an SESAM and an additional component in the cavity [23, 24]. In simulation, we will assume that the cavity contains not only an active mirror but also a dispersing interferometer with absorption. The dispersion factor is taken into account in the spectral domain by a standard procedure: using a transfer function. Thus, the initial spectral transfer function (4) takes the form

$$\tilde{A}_{out}(\omega) = \tilde{A}_{in}(\omega) \times \exp\{-i[\Phi_g(\omega) + \Phi_a(\omega)]\}\exp[-(\omega - \omega_0)^2/\omega_g^2], \quad (9)$$

where $\Phi_g(\omega)$ and $\Phi_a(\omega)$ are the phase characteristics of an active and an absorbing Gires–Tournois interferometer. We call attention to the fact that, in contrast to previous studies [10, 13, 14], dispersion characteristics in our model are taken into account through an additional phase change, without introducing tentative cavity dispersion and TOD into the model. This allows us to take into account the frequency dependence of the cavity dispersion within the spectrum of the pulse and obtain more accurate results, in particular to adequately assess the role of the asymmetry of the phase shift due to the compensating interferometer.

In computer simulation, we used data on the structure of an active semiconductor mirror from Ref. [13]. A gain medium based on GaInAs quantum wells in a layer of thickness $2.75\lambda_0$ is located on a 100% Bragg reflector. The outer coating, of reflectivity $r_g = 0.4$, and the Bragg reflector form a microcavity. The resonance frequency of the microcavity is equal to the peak gain frequency ω_0 [13]. The gain coefficient is adjusted so that the amplitude gain is consistent with the values used in the simulation. The spectral dependences of dispersion $\beta_2(\lambda)$ thus obtained are shown in Figs 3a and 3c. The phase shift in the spectral range near ω_0 is almost linear and determines low values of dispersion and TOD. Dispersion $\beta_2(\lambda)$ is an odd function of ω_0 and its maximum value (in magnitude) is $\sim 3\times10^{-28}$ s^2. The maximum value (in magnitude) of TOD β_3 is about -1.5×10^{-41} s^3. These values correspond to known parameters of active semiconductor mirrors in disk lasers [12, 25].

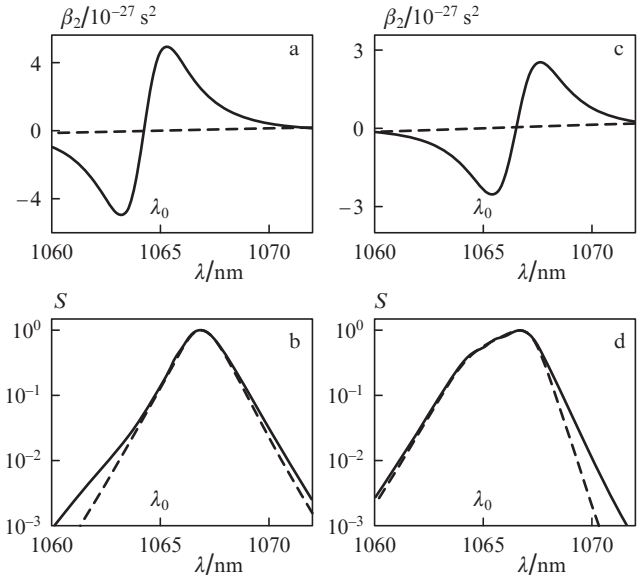

Figure 3. Spectral dependences of dispersion for absorbing Gires–Tournois interferometers that were used in simulation and ensure (a) normal and (c) anomalous dispersion (solid lines) and for an active mirror (dashed lines); (b, d) normalised $S(\lambda)$ spectra obtained for pulses by simulation using Gires–Tournois interferometers (solid lines) and at a constant cavity dispersion throughout the spectrum (dashed lines). Figure 3b corresponds to constant normal dispersion $\beta_2 = 4\times10^{-27}$ s^2 and an interferometer with characteristics presented in Fig. 3a, and Fig. 3d corresponds to constant anomalous dispersion $\beta_2 = -2\times10^{-27}$ s^2 and an interferometer with characteristics presented in Fig. 3c.

The dispersion characteristics of the absorbing mirror can also be calculated using (7) and (8). An important point is that the active and absorbing mirrors are adjusted to the same spectral range, so their dispersion characteristics vary over similar ranges. In the model under consideration, the zero dispersion (ω_2) frequencies of the active and absorbing mirrors (i.e. the resonance frequencies of the microcavities) differ by ω_r, which is determined by the characteristics of the absorbing mirror.

Figure 3a shows the spectral dependence of dispersion for an absorbing Gires–Tournois interferometer. Its parameters ($\omega_r = 6\times10^{12}$ s^{-1}; $r_g = 0.5$; thickness of the absorbing GaAs layer, $7.75\lambda_r$; absorption $a = 0.5$ dB) are chosen so that the interferometer has normal dispersion $\beta_2 \approx 4\times10^{-27}$ s^2 at the peak gain frequency ω_0. Note that the dispersion properties of the cavity in the model under consideration are completely determined by the parameters of the absorbing compensator. The dispersion set by it is sufficient for reducing nonlinear FM, as can be seen from the spectral shape of the pulse (Fig. 3b). Its spectrum has an almost symmetric shape, corresponding to a pulse with no FM. Significant deviations

from this shape occur only for $\beta_2(\lambda) < 0$. However, since the pulse power is low in this range, this leads to only slight FM at the edges of the pulse.

Figure 3c shows the spectral dependence $\beta_2(\lambda)$ for an absorbing Gires–Tournois interferometer that ensures anomalous cavity dispersion at wavelength λ_0. Its parameters ($\omega_r = -1.8\times10^{13}$ s^{-1}; $r_g = 0.5$; thickness of the absorbing GaAs layer, $5.75\lambda_r$; absorption $a = 0.3$ dB) ensure anomalous dispersion $\beta_2 \approx -2\times10^{-27}$ s^2 at frequency ω_0. The spectrum of the pulse in Fig. 3d leads us to conclude that nonmonotonic FM is mainly suppressed. Comparison with the spectrum obtained by simulation for a cavity with constant dispersion throughout the spectrum demonstrates that both pulses have negative FM (as evidenced by the sloping top of the spectrum, with its maximum shifted to longer wavelengths). The spectra differ markedly in the range where the dispersion of the compensating interferometer is $\beta_2(\lambda) > 0$. In this region, the negative FM of the pulse generated in the cavity with a Gires–Tournois interferometer is weaker than that of the control pulse. At the trailing edge of the pulse, where its power is rather low, a small region of positive FM may be observed. The envelopes of the pulses, the time dependences of their instantaneous frequency and the corresponding spectral characteristics are presented in Figs 4b, 4e [for normal dispersion of the absorbing interferometer at the peak gain wavelength: $\beta_2(\lambda_0) > 0$], 5b and 5e [for anomalous dispersion: $\beta_2(\lambda_0) < 0$].

Clearly, when Gires–Tournois interferometers are used as dispersion compensators, important parameters are not only $\beta_2(\lambda_0)$ but also the width of the spectral range where the sign of the dispersion of the interferometer remains unchanged. To a first approximation, this width is determined by the maximum rate of the variation in the dispersion of the interferometer with wavelength, i.e. by the maximum TOD value. This value is reached at the wavelength corresponding to the shift frequency $\omega_0 + \omega_r$. Figures 4 and 5 present simulation results for a disk laser with a Gires–Tournois interferometer as a dispersion compensator, which has various maximum values of TOD, but with $\beta_2(\lambda_0)$ remaining unchanged.

Our results demonstrate that, at a high maximum TOD value, which characterises an interferometer with dispersion parameters rapidly varying over the spectrum, the alternating-sign FM of the pulse being generated is not completely compensated. In the case of normal dispersion, $\beta_2(\lambda_0) > 0$ (Figs 4a, 4d), FM is only compensated near the pulse maximum, whereas regions of alternating-sign FM are observed at the edges of the pulse. In the case of anomalous dispersion, $\beta_2(\lambda_0) < 0$ (Figs 5a, 5d), the cavity dispersion is insufficient for obtaining negative FM throughout the pulse. As a result, an asymmetric tail can be seen at the trailing edge of pulses. Its formation is related to nonmonotonic-FM filtration and the absorption saturation region behind the pulse. The pulse envelope varies with time in both instances (see Section 2). Alternating-sign FM distorts the spectrum of the pulse in both instances: its shape also varies with time. The presence of several peaks is due to the fact that the envelope has several local maxima.

An increase in the range where the sign of the dispersion of the interferometer remains unchanged (i.e. a reduction in its maximum TOD) is accompanied by positive trends in the formation of the envelope and spectrum of the pulse. As a boundary, we can tentatively take the maximum TOD $\beta_3' = \beta_2^{max}/\Delta\omega$, where β_2^{max} is the maximum value (in magnitude) of the interferometer dispersion and $\Delta\omega$ is the spectral width of the pulse, which depends on gain, gain bandwidth and gain

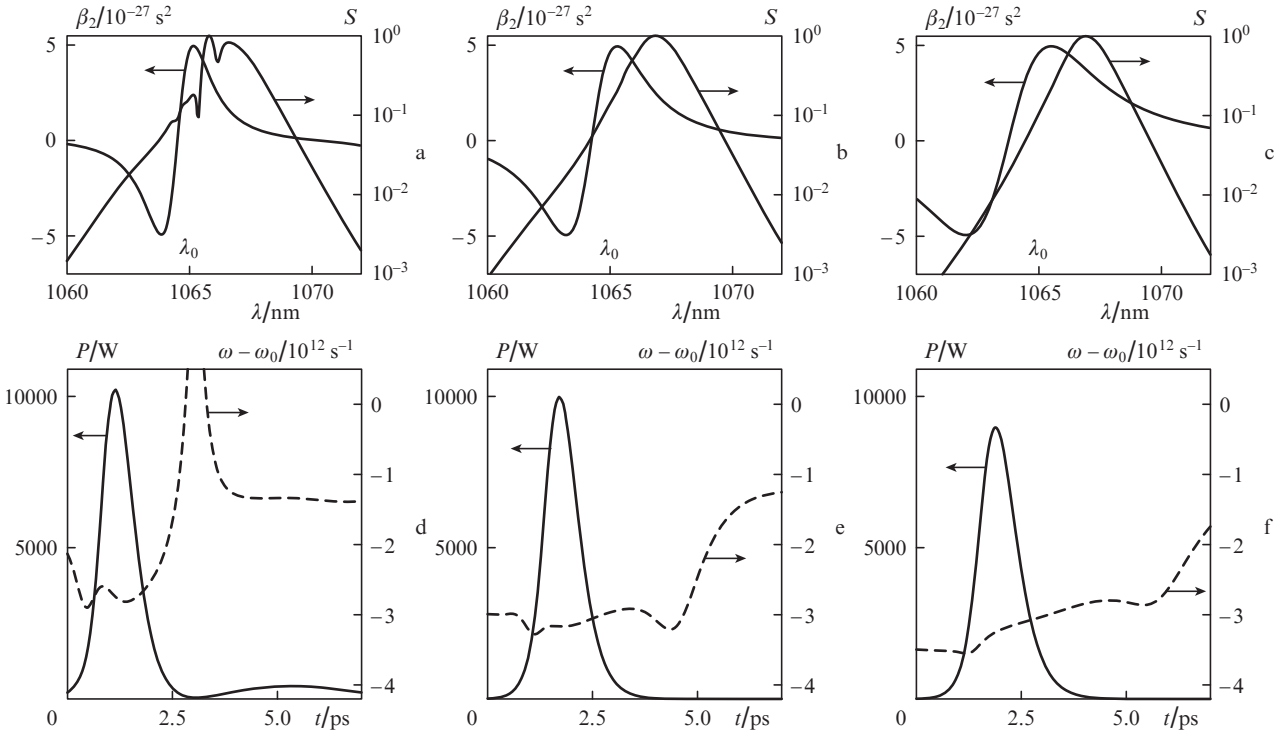

Figure 4. (a–c) Spectral dependences $\beta_2(\lambda)$ for a Gires–Tournois interferometer that is used for dispersion compensation [normal dispersion $\beta_2(\lambda_0) \approx 4\times10^{-27}$ s^2] and the corresponding normalised spectra $S(\lambda)$ of disk laser pulses; (d–f) pulse envelopes and time dependences of the instantaneous pulse frequency for a disk laser with a Gires–Tournois interferometer as a dispersion compensator. The maximum TOD is $\beta_3 =$ (a, d) 6×10^{-39}, (b, e) 4×10^{-39} and (c, f) 1.5×10^{-39} s^3.

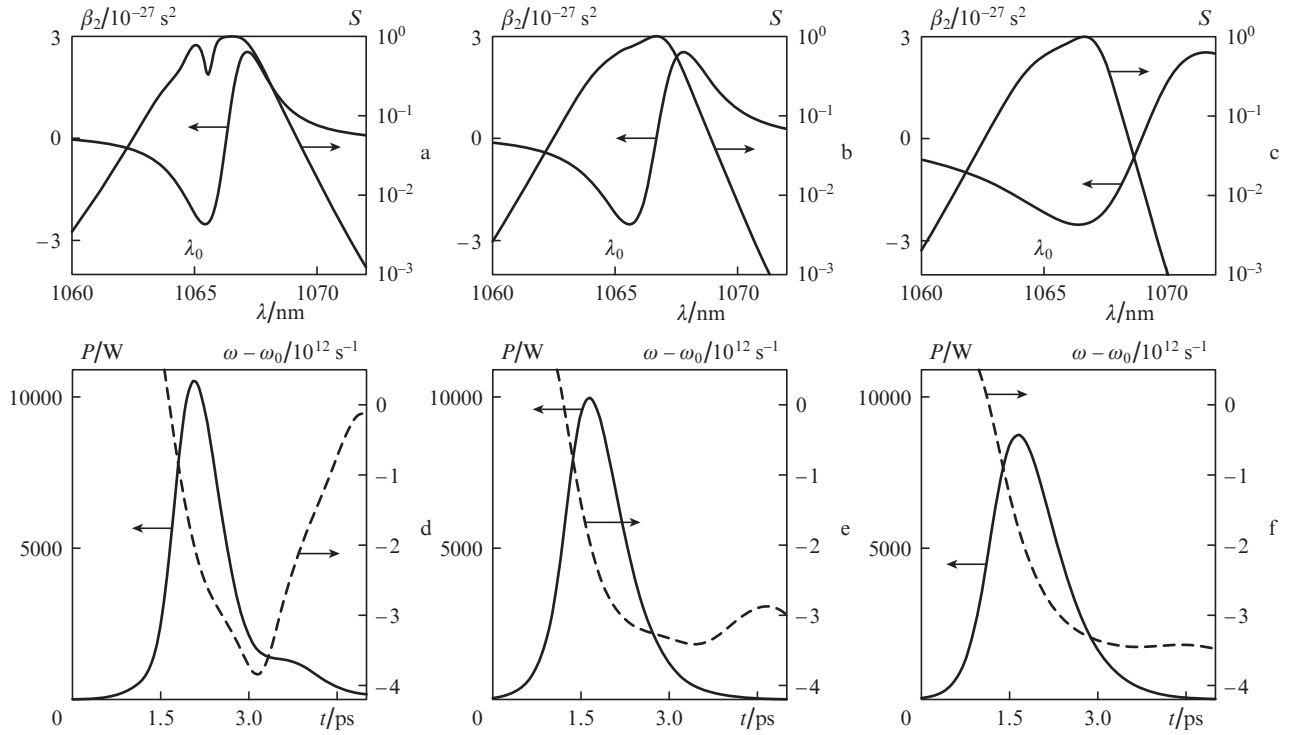

Figure 5. Same as in Fig. 4, but for anomalous dispersion $\beta_2(\lambda_0) = -2\times10^{-27}$ s^2. The maximum TOD is β_3 = (a, d) 3×10^{-39}, (b, e) 2.5×10^{-39} and (c, f) 10^{-39} s^3.

and absorption saturation and modulation parameters. In the model under consideration, $\beta_3' \approx 5\times10^{-39}$ s^3 for an interferometer with $\beta_2(\lambda_0) > 0$, and $\beta_3' \approx 2.7\times10^{-39}$ s^3 for an interferometer with $\beta_2(\lambda_0) < 0$. If the maximum TOD is lower than β_3' (Figs 4b, 4c, 4e, 4f, 5b, 5c, 5e, 5f), as a result of FM stabilisation the envelope and spectrum of the pulse become time-independent. For $\beta_2(\lambda_0) > 0$ and a TOD slightly lower than the limiting value β_3' (Figs 5b, 5e), FM is essentially constant along the pulse: a transform-limited pulse is generated. Spectral filtration of the gain ensures a stable envelope shape. For interferometers with a low maximum TOD (Figs 4c, 4f), the carrier frequency of pulses shifts to longer wavelengths, which is due to the presence of a broad spectral range of anomalous dispersion for $\lambda < \lambda_0$. It is also worth noting the weak positive FM of the pulse. This is due to a standard dispersion effect and leads to a decrease in pulse peak power and an increase in pulse duration.

Analogous results can be obtained for anomalous dispersion (Fig. 5). An important feature of nonmonotonic-FM compensation using an anomalous dispersion [$\beta_2(\lambda_0) < 0$] interferometer is the strong residual negative FM, which is almost linear over most of the pulse. Even though this FM is asymmetric with respect to the pulse 'axis', which passes through the maximum in the envelope, it offers the possibility of rather effective pulse compression using an external dispersing component, e.g. a prism or a normal dispersion ($\beta_2 > 0$) diffraction grating pair. Figure 6 presents simulation results for the compression of a pulse obtained in the cavity of a disk laser with an anomalous dispersion [$\beta_2(\lambda_0) < 0$] interferometer using a normal dispersion external component (for simplicity, we consider the case where higher orders of dispersion in this component are negligible). It is seen that, after compression, the peak power of the pulse represented in Fig. 5f can be considerably increased (by more than a factor of 1.5). Note that

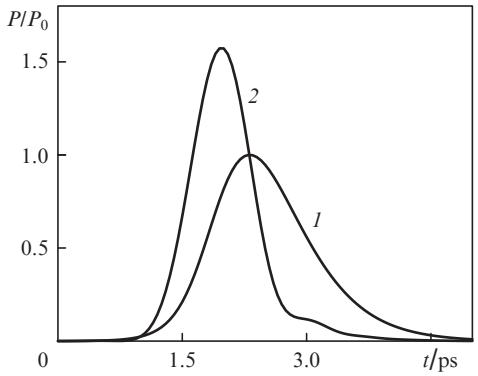

Figure 6. (*1*) Envelope of an output disk laser pulse in simulation with an anomalous dispersion [$\beta_2(\lambda_0) < 0$] Gires–Tournois interferometer; (*2*) envelope of the pulse obtained by output pulse compression using a normal dispersion diffraction grating pair with $\beta_2 = 3\times10^{-25}$ s^2.

FM asymmetry leads to an asymmetric shape of the envelope of the compressed pulse.

5. Conclusions

We have examined a numerical model for a semiconductor disk laser mode-locked by an SESAM semiconductor mirror. The model takes into account nonlinear gain and absorption saturation effects in the semiconductor, including phase modulation, which leads to pulse FM. The rate and sign of the FM depend on saturable absorption and saturated gain parameters and phase modulation depth. It has been shown that a disk laser pulse may have either monotonic or alternating-sign FM, depending on the gain bandwidth. In the latter case, the envelope and spectrum of the pulse are time-dependent.

We have studied the effect of second-order cavity dispersion β_2 on pulse FM. The results demonstrate that, at a certain normal dispersion, pulses generated in the cavity are similar in characteristics to a transform-limited soliton pulse. In the case of anomalous dispersion, pulses have negative FM, and the anomalous dispersion required to suppress alternating-sign FM is lower than the normal dispersion needed for this purpose.

We have examined the possibility of tuning the dispersion properties of a cavity using an absorbing Gires–Tournois interferometer with different signs of detuning of its resonance frequency ω_r from the peak gain frequency ω_0. For this purpose, use can be made of both an SESAM with optimised characteristics and a specially designed dispersion compensator. It has been shown that alternating-sign FM can be effectively suppressed by limiting the maximum TOD of the compensating interferometer. The limiting TOD value is determined by the necessary β_2 dispersion and the pulse bandwidth. It has also been shown that the use of a low-TOD compensating interferometer leads to dispersion-induced pulse broadening and a decrease in pulse peak power.

The proposed model and present results may be helpful in calculating cavities and optimising parameters of disk lasers. Moreover, the model for an absorbing Gires–Tournois interferometer can be used for controlling the dispersion characteristics of SESAM semiconductor mirrors, which are widely used in various areas of laser engineering.

Acknowledgements. This work was supported by the RF Ministry of Education and Science (Project No. 14.Z50.31.0015, State Research Task).

References

1. Okhotnikov O.G. (Ed.) *Semiconductor Disk Lasers. Physics and Technology* (Weinheim: Wiley-VCH, 2010).
2. Baer C., Heckl O., Saraceno C., Schriber C., Krankel C., Sudmeyer T., Keller U. *Opt. Express*, **20**, 7054 (2012).
3. Keller U., Tropper A.C. *Phys. Rep.*, **429**, 67 (2006).
4. Scheller M., Wang T.L., Kunert B., Stolz W., Koch S.W., Moloney J.V. *Electron. Lett.*, **48** (10), 588 (2012).
5. Wilcox K.G., Quarterman A.H., Apostolopoulos V., Beere H.E., Farrer I., Ritchie D.A., Tropper A.C. *Opt. Express*, **20** (7), 7040 (2012).
6. Klopp P., Griebner U., Zorn M., Weyers M. *Appl. Phys. Lett.*, **98** (7), 071103 (2011).
7. Okhotnikov O.G. *Kvantovaya Elektron.*, **38**, 1083 (2008) [*Quantum Electron.*, **38**, 1083 (2008)].
8. Keller U., Weingarten K.J., Kartner F.X., Kopf D., Braun B., Jung I.D., Fluck R., Honninger C., Matuschek N., Aus der Au J. *IEEE J. Sel. Top. Quantum Electron.*, **2** (3), 435 (1996).
9. Zhang Q., Jasim K., Nurmikko A.V., Mooradian A., Carey G., Ha W., Ippen E. *IEEE Photonics Technol. Lett.*, **16**, 885 (2004).
10. Saarinen E.J., Härkönen A., Herda R., Suomalainen S., Orsila L., Hakulinen T., Guina M., Okhotnikov O.G. *Opt. Express*, **15**, 955 (2007).
11. Lozano C., García-Fernández P., Mirasso C.R. *Opt. Commun.*, **123** (4), 752 (1996).
12. Jiang W., Derickson D.J., Bowers J.E. *IEEE J. Quantum Electron.*, **29** (5), 1309 (1993).
13. Saarinen E., Herda R., Okhotnikov O. *J. Opt. Soc. Am. B*, **24**, 2784 (2007).
14. Paschotta R., Häring R., Garnache A., Hoogland S., Tropper A.C., Keller U. *Appl. Phys. B*, **75**, 445 (2002).
15. Henry C.H. *IEEE J. Quantum Electron.*, **18** (2), 259 (1982).
16. Agrawal G.P., Bowden C.M. *IEEE Photonics Technol. Lett.*, **5** (6), 640 (1993).
17. Isomäki A., Okhotnikov O.G. *Opt. Express*, **14** (10), 4368 (2006).
18. Fork R., Martinez O., Gordon J. *Opt. Lett.*, **9**, 150 (1984).
19. Tempea G., Krausz F., Spielmann C., Ferencz K. *IEEE J. Sel. Top. Quantum Electron.*, **4** (2), 193 (1998).
20. Gires F., Tournois P. *C. R. Acad. Sci. Paris*, **258**, 6112 (1964).
21. Akhmanov S.A., Vysloukh V.A., Chirkin A.S. *Optics of Femtosecond Laser Pulses* (New York: Am. Inst. of Physics, 1992; Moscow: Nauka, 1988).
22. Zolotovskii I.O., Korobko D.A., Ostatochnikov V.A. *Kvantovaya Elektron.*, **45** (2), 136 (2015) [*Quantum Electron.*, **45** (2), 136 (2015)].
23. Isomaki A., Vainionpaa A., Lyytikainen J., Okhotnikov O.G. *Appl. Phys. Lett.*, **82** (17), 2773 (2003).
24. Kopf D., Zhang G., Fluck R., Moser M., Keller U. *Opt. Lett.*, **21** (7), 486 (1996).
25. Laporta P., Magni V. *Appl. Opt.*, **24**, 2014 (1985).